Bull. Mater. Sci., Vol. 39, No. 6, October 2016, pp. 1381–1387. © Indian Academy of Sciences.
DOI 10.1007/s12034-016-1279-7

Rose bengal-sensitized nanocrystalline ceria photoanode for dye-sensitized solar cell application

SUHAIL A A R SAYYED[1,2], NIYAMAT I BEEDRI[1], VISHAL S KADAM[1] and HABIB M PATHAN[1,*]

[1]Advanced Physics Laboratory, Department of Physics, Savitribai Phule Pune University, Pune 411 007, India
[2]Department of Physics, B.P.H.E. Society's Ahmednagar College, Ahmednagar 414001, India

MS received 24 April 2015; accepted 21 March 2016

Abstract. **For efficient charge injection and transportation, wide bandgap nanostructured metal oxide semiconductors with dye adsorption surface and higher electron mobility are essential properties for photoanode in dye-sensitized solar cells (DSSCs). TiO_2-based DSSCs are well established and so far have demonstrated maximum power conversion efficiency when sensitized with ruthenium-based dyes. Quest for new materials and/or methods is continuous process in scientific investigation, for getting desired comparative results. The conduction band (CB) position of CeO_2 photoanode lies below lowest unoccupied molecular orbital level (LUMO) of rose bengal (RB) dye. Due to this, faster electron transfer from LUMO level of RB dye to CB of CeO_2 is facilitated. Recombination rate of electrons is less in CeO_2 photoanode than that of TiO_2 photoanode. Hence, the lifetime of electrons is more in CeO_2 photoanode. Therefore, we have replaced TiO_2 by ceria (CeO_2) and expensive ruthenium-based dye by a low cost RB dye. In this study, we have synthesized CeO_2 nanoparticles. X-ray diffraction (XRD) analysis confirms the formation of CeO_2 with particle size ∼7 nm by Scherrer formula. The bandgap of 2.93 eV is calculated using UV–visible absorption data. The scanning electron microscopy (SEM) images show formation of porous structure of photoanode, which is useful for dye adsorption. The energy dispersive spectroscopy is in confirmation with XRD results, confirming the presence of Ce and O in the ratio of 1:2. UV–visible absorption under diffused reflectance spectra of dye-loaded photoanode confirms the successful dye loading. UV–visible transmission spectrum of CeO_2 photoanode confirms the transparency of photoanode in visible region. The electrochemical impedance spectroscopy analysis confirms less recombination rate and more electron lifetime in RB-sensitized CeO_2 than TiO_2 photoanode. We found that CeO_2 also showed with considerable difference between dark and light DSSCs performance, when loaded with RB dye. The working mechanism of solar cells with fluorine-doped tin oxide (FTO)/CeO_2/RB dye/carbon-coated FTO is discussed. These solar cells show V_{OC} ∼360 mV, J_{SC} ∼0.25 mA cm^{-2} and fill factor ∼63% with efficiency of 0.23%. These results are better as compared to costly ruthenium dye-sensitized CeO_2 photoanode.**

Keywords. **Wide bandgap; dye-sensitized solar cells; CeO_2; rose bengal dye.**

1. Introduction

The sun annually supplies about 3×10^{24} J energy to the earth, which is about 10,000 times more than the global population that currently consumes [1]. The power reaching earth from the sun is 1.37 kW m^{-2}, which is free of cost. Since couple of decades, it has become possible to capture the sunlight and turn it into electric power or to generate chemical fuels, such as hydrogen, using advanced technologies. The photovoltaic market is still dominated by conventional semiconductor solar cells, which are expensive. Although photovoltaic technology can provide clean and renewable energy, its high-cost production and installation excludes direct commercial use. It is an urgent requirement to develop cheaper photovoltaic devices with moderate efficiency. DSSC is a promising alternative to conventional semiconductor solar cells, because of low-fabrication cost. DSSCs have attracted great interest in recent years due to high performance, simple manufacturing process, high flexibility, semi-transparency, environmental friendliness, high efficiency and low cost etc [2].

Commonly TiO_2 is widely considered photoanode material in DSSC application due to non-toxic and chemical stability properties. DSSCs with functioning components of photoanode (TiO_2), dye molecule (ruthenium-based N3 or N719), electrolyte (I^-/I_3^- as redox electrolyte) and counter electrode (Pt-coated) demonstrated nearly 12% power conversion efficiency [3]. Metal oxides such as ZnO [4–7], Nb_2O_5 [8,9], CeO_2 [10] and SnO_2 [11,12] have also been used as alternative photoanode with spherical morphologies in DSSCs. Nair *et al* [13] studied the effect of TiO_2 nanotube length and lateral tubular spacing on photovoltaic properties of back illuminated DSSCs. Cyriac *et al* [14] developed a new type of solid-state absorber material for DSSCs. Rajkumar *et al* [15] developed hybrid nanocrystalline TiO_2 solar cell with copper phthalocyanine as

*Author for correspondence (pathan@physics.unipune.ac.in)

sensitizer and hole transporter. Baviskar *et al* [16] discussed influence of different processing parameters on chemically grown ZnO films with low-cost Eosin–Y dye for DSSCs. Great efforts are being focused on the development of DSSCs with semiconductor photoanode as replacement to TiO_2 and organic dyes as the sensitizer [17–19]. Researchers have used CeO_2 along with TiO_2 or ZnO as photoanode, either to suppress the recombination rate or as a mirror-like coating for absorption of maximum photons by dye [20–26]. There are few reports of directly using CeO_2 as photoanode in DSSCs [10]. The CB position of CeO_2 is below the lowest unoccupied molecular orbital (LUMO) level of most of the dyes (also RB dye) [27,28]. The recombination rate of electrons is less and hence higher electron lifetime in CeO_2 than TiO_2 [29]. CeO_2 is non-toxic and chemically stable. The conductivity of CeO_2 varies from 0.1 to 77×10^{-6} S cm^{-1} depending upon the methods of synthesis, doping and conditions of testing [30,31]. Hence, CeO_2 can be considered as a potential candidate for photoanode in DSSCs.

In this study, we have replaced TiO_2 by CeO_2 and ruthenium-based dye with cost-effective RB dye. CeO_2 nanoparticles were synthesized using simple precipitation method. Initially CeO_2 nanocrystalline powder/photoanode was characterized by X-ray diffraction (XRD), scanning electron microscopy (SEM), energy dispersive spectroscopy (EDS), UV–visible spectroscopy (absorption and transmission) and electrochemical impedance spectroscopy (EIS) for its structure, morphology, composition, bandgap and bode plot etc. and then envisaged in DSSCs application. RB dye was characterized using UV–visible absorption spectroscopy. DSSCs were fabricated and photocurrent density–voltage (J–V) characteristics were studied to check the performance.

2. Experimental

2.1 *Materials*

Cerium nitrate ($Ce(NO_3)_3{\cdot}6H_2O$) purchased from HPLC and ammonium hydroxide solution (20%, NH_4OH) purchased from Thomas Baker were used for synthesis of CeO_2 nanoparticles. RB dye purchased from HPLC was used for sensitization of photoanode. Standard iodine solution was used as electrolyte.

2.2 *Synthesis of CeO_2 nanoparticles*

The synthesis of CeO_2 nanoparticles by precipitation method has been discussed by different researchers [20,32,33]. The nanocrystalline CeO_2 powder was prepared using $Ce(NO_3)_3{\cdot}6H_2O$ and NH_4OH, where $Ce(NO_3)_3{\cdot}6H_2O$ was used as a source of Ce^{4+} and NH_4OH was the precipitant.

In a typical synthesis, 0.1 M $Ce(NO_3)_3{\cdot}6H_2O$ was prepared in double-distilled water under constant stirring at room temperature, then 20 ml of 20% NH_4OH solution was added drop-wise. The final product was kept in an incubator till the water evaporated and the nanaocrystalline CeO_2 powder was collected. This powder was annealed at 450°C. The crystal structure of the sample was identified using XRD (model no. D-8 Advance Bruker AXS, Germany) equipped with a monochromator CuKα radiation source ($\lambda = 1.54$ Å).

2.3 *CeO_2 electrode fabrication*

To make CeO_2 paste, 0.5 g of the above-prepared CeO_2 powder was mixed with 0.4 g ethyl cellulose, 2.5 g anhydrous terpineol and 5 ml ethyl alcohol. The mixture was properly mixed using mortar and pestle to form a uniform jelly-like paste, which is then ultra-sonicated for 1 h. Later, this paste was deposited on fluorine-doped tin oxide (FTO) glass using doctor-blade method. After few minutes of drying, electrode was kept for annealing at 450°C for 1 h and then characterized by SEM (JEOL-JSM 6360-A), UV–vis absorption under diffused reflectance spectra and transmission spectra (Jasco, model: V-670).

2.4 *Sensitization of CeO_2 electrode*

Annealed CeO_2 electrodes were immersed into 0.3 mM RB dye for 24 h to adsorb dye. The absorption spectrum of RB dye and dye-loaded photoanode was recorded by UV–vis spectrophotometer in the range of 200–800 nm to study its optical properties.

2.5 *Preparation of counter electrode*

To prepare counter electrode, the FTO glass was washed with acetone, water and ethanol. After removing contaminants, carbon-coated counter electrode was prepared on the conductive side of the FTO substrate by using mild flame of candle.

2.6 *Fabrication of DSCCs*

To fabricate the DSSCs, few drops of electrolyte solution (iodine) were added to dye-loaded CeO_2 photoanode before covering the substrate with counter electrode (carbon-coated FTO). Then, both the photoanode and the counter electrode were clamped together. Later, J–V characteristics of these solar cells were studied.

3. Results and discussion

3.1 *XRD analysis*

As shown in figure 1, the XRD pattern of CeO_2 consists of eight peaks at $2\theta = 28.6$, 33.1, 47.5, 56.4, 59.1, 68.1, 76.8 and 79.1° corresponding to (111), (200), (220), (311), (222), (400), (331) and (420) planes of cubic structure of CeO_2, respectively, in accordance with Joint Committee on Powder Diffraction Standards (JCPDS no. 81-0792, ICSD#072155,

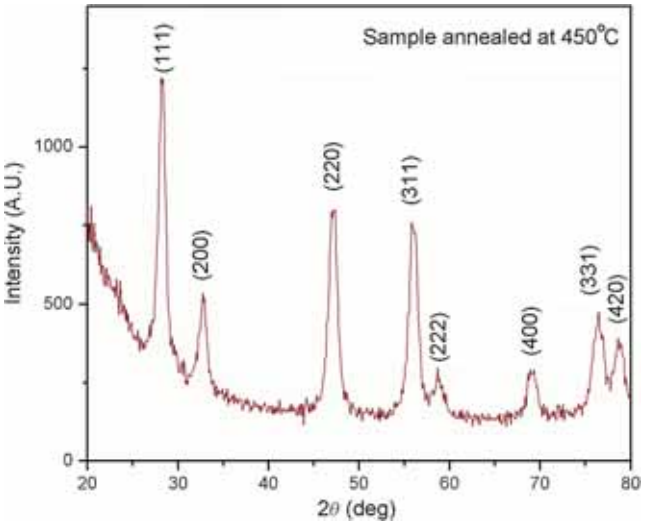

Figure 1. X-ray diffraction pattern of CeO_2 powder.

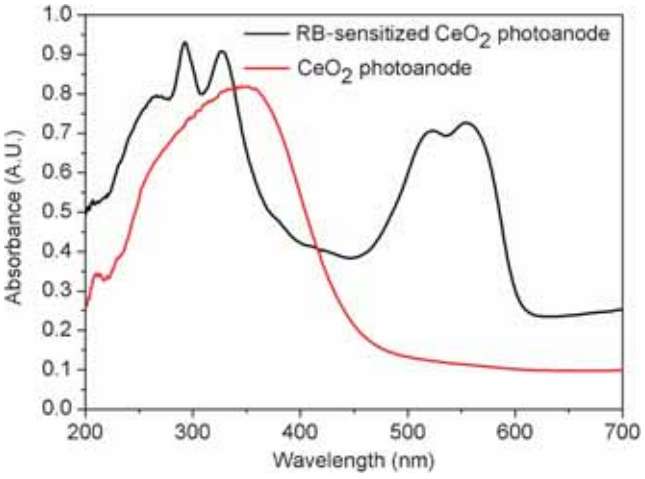

Figure 2. Optical absorption spectra of CeO_2 photoanode before and after sensitization with RB dye.

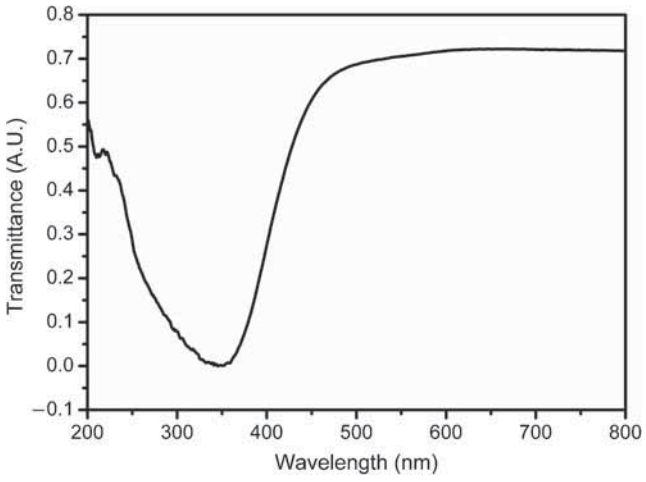

Figure 3. Optical transmittance spectra of CeO_2 photoanode.

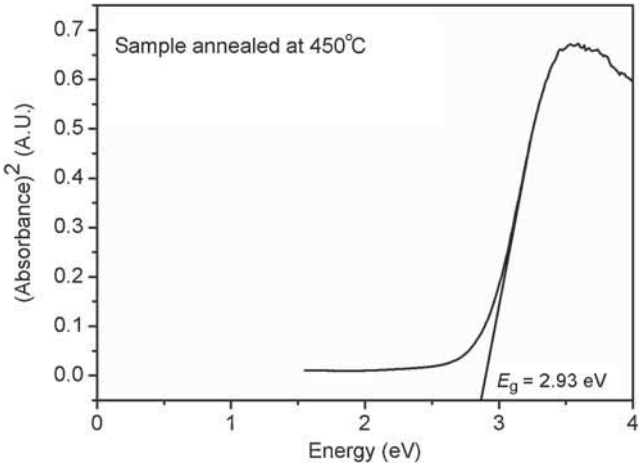

Figure 4. Bandgap energy calculation of CeO_2 photoanode.

space group: Fm3m (225), unit cell parameters: $a = b = c =$ 5.4124 Å). No diffraction peaks due to impurities, such as $Ce(OH)_2$, are found in XRD patterns.

The average particle size (D) of CeO_2 powder annealed at 450°C is estimated by using Debye-Scherrer formula [34].

$$D = \frac{0.89\lambda}{\beta \cos\theta}, \tag{1}$$

where λ is wavelength of CuKα = 1.54 Å, β the full-width in radians at half-maximum of diffraction peaks and θ the Bragg's angle of the X-ray pattern at maximum intensity. The estimated particle size is ∼7 nm for the annealed powder at 450°C.

3.2 *Optical properties of CeO_2*

As shown in figure 2, it is observed that the absorption is maximum for as-prepared CeO_2 film (annealed at 450°C) at ∼360 nm. It shows that dye is adsorbed on the CeO_2 photoanode. The transmittance ($\%T$) against wavelength graph, from figure 3, shows that there is transmission of all the wavelengths in visible range (400–800 nm). Hence complete visible spectrum is available for dye to absorb photons.

The absorption data obtained from UV–vis spectrophotometer are used to calculate the bandgap energy. As shown in figure 4, the bandgap of CeO_2 annealed at 450°C is found to be 2.93(±0.02) eV. However, the obtained bandgap is lower than the reported bandgap (3.2eV) of bulk CeO_2 [35].

It is well reported that, with decrease in size of crystal, the value of bandgap increases as an effect of quantum confinement [36]. In case of CeO_2, the presence of significant fraction of Ce atoms (in either 3+ or 4+ state) on the external surface leads to oxygen vacancies and defects, whose influence on the bandgap overcomes the expected influence of regular quantum size effect [29,37,38].

3.3 *Optical absorption spectra of RB dye*

Absorption spectrum for the RB dye is shown in figure 5. The value of λ_{max} is an important parameter as it indicates the possibilities of these molecular systems for considerable use as a functional material in DSSCs. The absorption spectrum of RB dye constitutes four major absorption peaks. The possible transitions are shown in figure 6. The three peaks are at shorter wavelength region (265, 326 and 342 nm) may be corresponding to π–π*, σ–π* and σ–σ* transitions. One peak at longer wavelength region (542 nm) may be due to intra-molecular charge transfer transitions from the donor to acceptor level with highest occupied molecular orbital (HOMO)–LUMO energy levels [39,40].

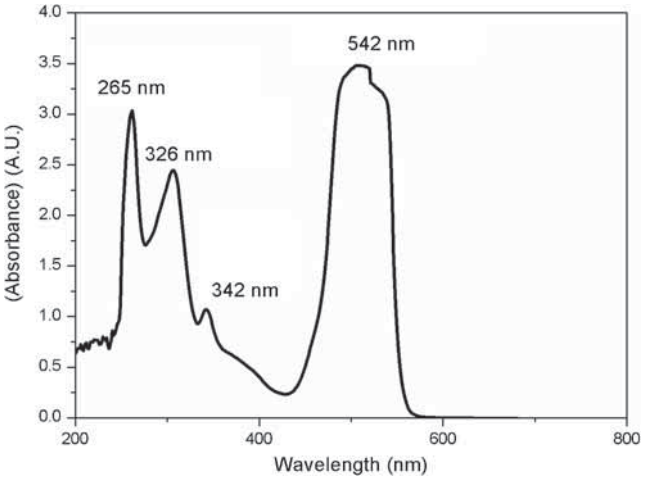

Figure 5. Optical absorption spectrum of RB dye.

3.4 *Surface morphology and EDS of CeO_2 film*

The SEM images shown in figure 7 are obtained to study the surface morphology of CeO_2 photoanode. The CeO_2 possesses network of aggregated spheres-like morphology with pore-size roughly in 60–80 nm range. The EDS of CeO_2 film is shown in figure 7. The peak heights for Ce and O are in the ratio of 1:2, confirming the presence of Ce and O in the ration of 1:2.

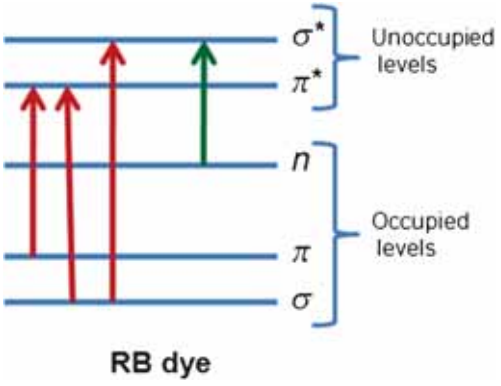

Figure 6. Possible transition mechanisms in RB dye.

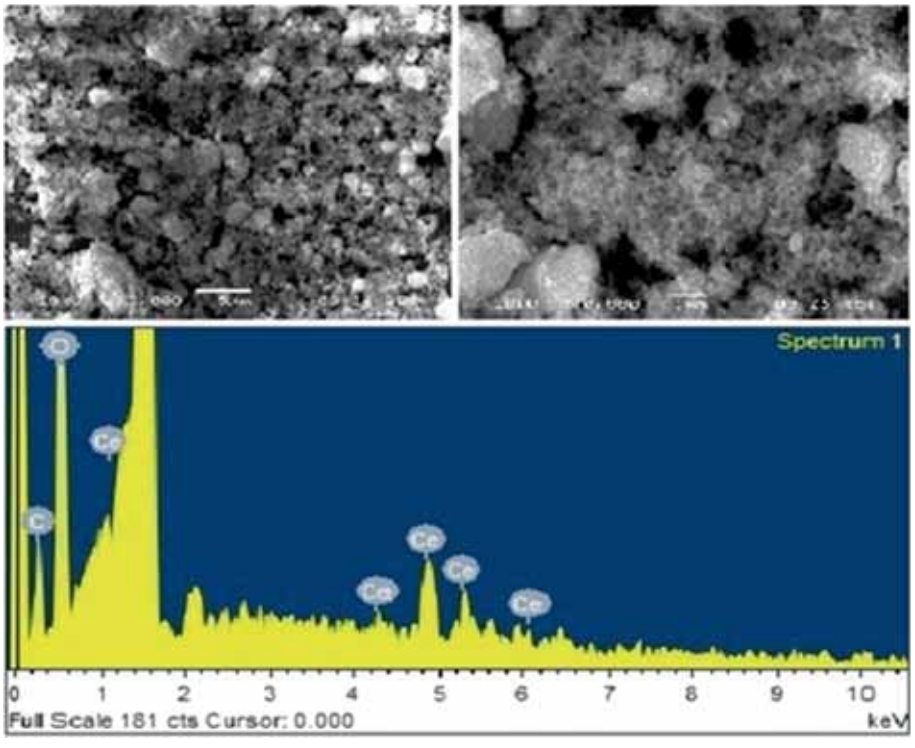

Figure 7. SEM images and EDS of CeO_2 photoanode.

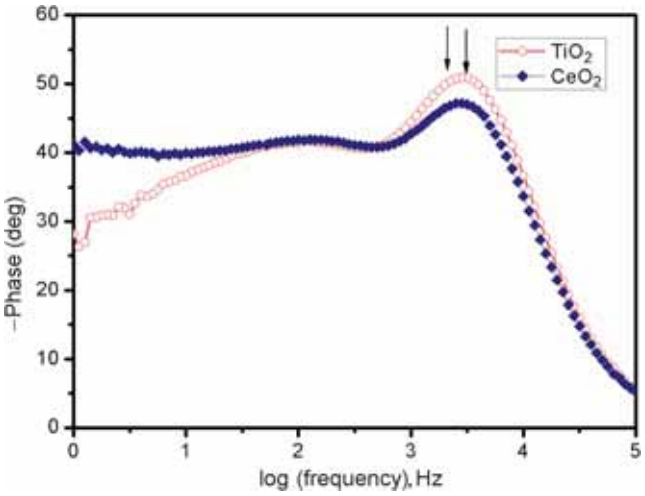

Figure 8. Bode plot for RB-sensitized TiO_2 and CeO_2 photoanode.

3.5 *EIS analysis*

Figure 8 shows the EIS analysis (Bode plot) for RB-sensitized CeO_2 and TiO_2 photoanode. For CeO_2 photoanode, there is slight negative shift in frequency as compared to TiO_2 photoanode. Thus, there is slight increase in lifetime of electrons in CeO_2 photoanode, confirming reduction in recombination reactions.

3.6 *Photovoltaic analysis*

Charge transfer process in DSSCs based on RB-sensitized CeO_2 photoanode can be explained in similar way as Arote *et al* [39]. Charge transfer process is shown in figure 9.

When the photons get absorbed by the RB sensitizer, electrons in HOMO level get transferred to excited state, i.e., LUMO level. As observed in figure 9, the CB position of CeO_2 (−0.53 eV) [27,29,37,38,41] (*vs.* normal hydrogen electrode (NHE)) lies below the LUMO level of RB dye (−0.96 eV) [28] (*vs.* NHE); hence, the electrons in LUMO of RB dye are injected quickly into the CB of CeO_2 and then finally get transferred to the FTO substrate, where they are utilized for the conduction. The corresponding mechanism of transportation of electrons is represented by equations (2) and (3).

$$D + h\nu \rightarrow D^*, \tag{2}$$

$$D^* \rightarrow D^0 + e^-(CB), \tag{3}$$

where D, D* and D^0 correspond to ground state, excited and oxidized molecules of RB dye, respectively. The injected electrons diffuse into CeO_2 porous network and transfer through external load towards counter electrode. The oxidized dye is quickly reduced back to its original state by reduced redox species (R_s) in the electrolyte, which in turn becomes the oxidized redox species (R_s^0).

$$D^0 + R_s \rightarrow D + R_s^0, \tag{4}$$

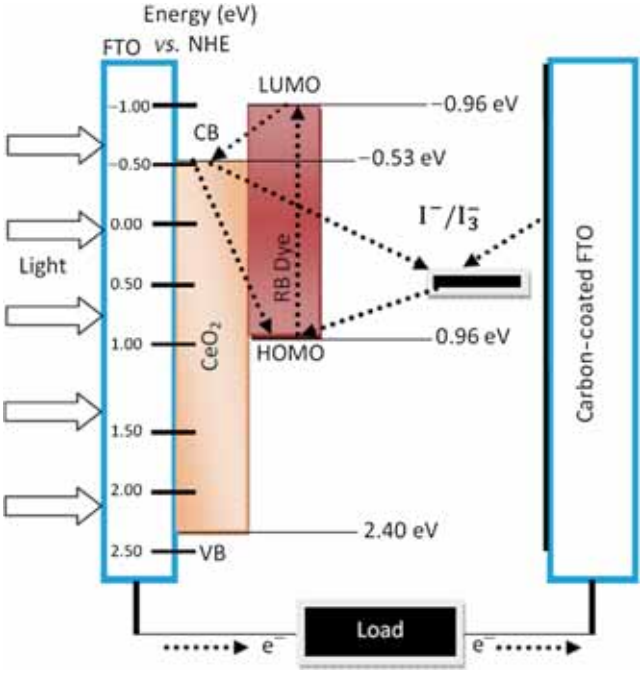

Figure 9. Schematic of processes involved in RB-sensitized CeO_2-based DSSCs.

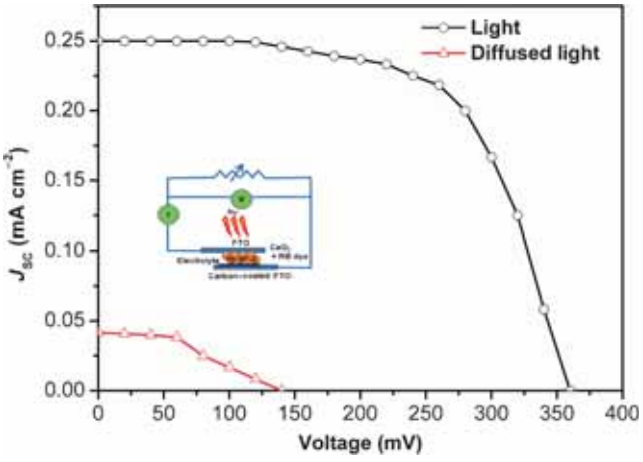

Figure 10. *J–V* characteristics of DSSCs based on RB CeO_2 photoanode.

where R_s and R_s^0 are the redox and oxidized species, respectively. This equation is generally called as dye regeneration process. Next, R_s^0 reduce back to the R_s by accepting electrons from counter electrode, in this way the electrons cycle gets complete.

3.7 *Cell performance analysis*

Figure 10 shows the *J–V* characteristics of DSSCs based on CeO_2 photoanode sensitized with RB dye. The dye adsorption time was optimized as 24 h. The cell area of 0.12 cm^2 was used. The cell performance was observed under light (25 mW cm^{-2}) and diffused light (2 mW cm^{-2}). The solar

Table 1. Solar cell parameters.

Condition	Light*	Diffused light**
V_{OC} (mV)	360	140
I_{SC} (mA)	0.030	0.005
V_{max} (mV)	260	60
I_{max} (mA)	0.026	0.0046
J_{SC} (mA cm^{-2})	0.25	0.0417
Cell area (cm^2)	0.12	0.12
Efficiency	0.23%	0.12%
Fill factor	63.07%	39.42%

*Light: 25 mW cm^{-2}, **diffused light: 2 mW cm^{-2}.

cell performance is listed in table 1. Under light, the solar cells show V_{oc} and J_{sc} values of about 360 mV and 0.25 mA cm^{-2}, respectively, with 0.23% efficiency and fill factor (FF) ∼63%. We observed better performance of the cells as compared to Turkovic and Crnjak [10], in which they noticed V_{OC} ∼60 mV and J_{SC} ∼25 mA cm^{-2} for costly ruthenium dye-sensitized CeO_2 photoanode.

4. Conclusion

In this study, the CeO_2 nanoparticles were successfully synthesized using chemical precipitation method having nanocrystalline size ∼7 nm. The CeO_2 films were prepared using doctor-blade method. The SEM shows that the porous structure is useful in DSSCs with bandgap of 2.93 eV, confirmed by UV–visible absorption data. The UV–visible absorption curve of RB-sensitized CeO_2 photoanode confirms adsorption of dye. The transparency of CeO_2 photoanode is confirmed by UV–visible optical transmittance spectra. The recombination rate of electrons is reduced in RB-sensitized CeO_2 than RB-sensitized TiO_2 photoanode. Hence, there is increase in electron lifetime in RB-sensitized CeO_2 photoanode. The photovoltaic performance of cells comprising of FTO/CeO_2/RB dye/carbon-coated FTO shows the open circuit voltage V_{oc} of 360 mV and photocurrent density J_{SC} of 0.25 mA cm^{-2} with efficiency ∼0.23% and FF ∼63%. These results are better as compared with costly ruthenium-sensitized CeO_2 photoanode.

Acknowledgements

We are grateful to the Board of College and University Development (BCUD), Savitribai Phule Pune University, Pune, for financial support through the minor research project OSD/BCUD/360/36. SAS is thankful to the Principal, Dr R J Barnabas, B.P.H.E. Society's Ahmednagar College, Ahmednagar, for kind support and constant motivation.

References

[1] Lewis N S 2007 *Science* **315** 798
[2] O'Regan B and Grätzel M 1991 *Nature* **353** 737
[3] Gao F, Wang Y, Shi D, Zhang J, Wang M, Jing X, Humphry-Baker R, Wang P, Zakeeruddin S M and Gratzel M 2008 *J. Am. Chem. Soc.* **130** 10720
[4] Singh R G, Gautam N, Gautam S K, Kumar V, Kapoor A and Singh F 2013 *J. Renew. Sust. Energy* **5** 033134(1–8)
[5] Khadtare S S, Jadkar S R and Pathan H M 2012 *Int. J. Green Nanotechnol.* **4** 528
[6] Khadtare S S, Ware A P, Gawali S S, Jadkar S R, Pingale S S and Pathan H M 2015 *RSC Adv.* **5** 17647
[7] Kumar V, Singh N, Kumar V, Purohit L P, Kapoor A, Ntwaeaborwa O M and Swart H C 2013 *J. Appl. Phys.* **114** 134506(1–6)
[8] Sayama K, Sugihara H and Arakawa H 1998 *Chem. Mater.* **10** 3825
[9] Lenzmann F, Krueger J, Burnside S, Brooks K, Gra M, Gal D, Ru S and Cahen D 2001 *J. Phys. Chem. B* **105** 6347
[10] Turkovic A and Crnjak Z 1997 *Sol. Energy Mater. Sol. Cells* **45** 275
[11] Chappel S and Zaban A 2002 *Sol. Energy Mater. Sol. Cells* **71** 141
[12] Shang G, Wu J, Huang M, Lin J, Lan Z, Huang Y and Fan L 2012 *J. Phys. Chem. C* **116** 20140
[13] Nair S V, Balakrishnan A, Subramanian K R V, Anu A M, Asha A M and Deepika B 2012 *Bull. Mater. Sci.* **35** 489
[14] Cyriac S L, Deepika B, Pillai B, Nair S V and Subramanian K R V 2014 *Bull. Mater. Sci.* **37** 685
[15] Sharma Rajkumar G D and Roy M S 2011 *Indian J. Pure Appl. Phys.* **49** 557
[16] Baviskar P, Ennaoui A and Sankapal B R 2014 *Solar Energy* **105** 445
[17] Sharma G D, Singh S P, Nagarjuna P, Mikroyannidis J A, Ball R J and Kurchania R 2013 *J. Renew. Sust. Energy* **5** 043107 (1–7)
[18] Hamann T W, Jensen R A, Martinson A B F, Ryswyk H V and Hupp J T 2008 *Energy Environ. Sci.* **1** 66
[19] Mishra A, Fischer M K R and Bauerle P 2009 *Angew. Chem. Int. Ed.* **48** 2474
[20] Sayyed S A A R, Beedri N I, Kadam V S and Pathan H M 2016 *Appl. Nanosci.* **6** 875
[21] Tripathi M and Chawla P 2014 *Ionics* **21** 541
[22] Rai P, Khan R, Ko K J, Lee J H and Yu Y T 2014 *J. Mater. Sci.: Mater. Electron* **25** 2872
[23] Lira-Cantu M and Krebs F C 2006 *Sol. Energy Mater. Sol. Cells* **90** 2076
[24] Upadhyay R, Tripathi M, Chawla P and Pandey A 2014 *J. Solid State Electrochem.* **18** 1889
[25] Hua Y, Yang B, Xu Z, Fengqui T, Max L G Q and Lianzhou W 2012 *Chem. Commun.* **48** 7386
[26] Roh J, Hwang S H and Jang J 2014 *ACS Appl. Mater. Interfaces* **6** 19825
[27] Elaziouti A, Laouedj N, Bekka A and Vannier R N 2014 *Sciences Technologie A* **39** 9
[28] Pradhan B, Batabyal S K and Pal A J 2007 *Sol. Energy Mater. Sol. Cells* **91** 769
[29] Corma A, Atienzar P, Garcia H and Chane-Ching J 2004 *Nat. Mater.* **3** 394
[30] Fan L, Ma Y, Wang X, Singh M and Zhu B 2014 *J. Mater. Chem. A* **2** 5399

[31] Shehata N, Clavel M, Meehan K, Samir E, Soha Gaballah and Salah M 2015 *Materials* **8** 7663

[32] Godinho M J, Gonçalves R F, Santos L P S, Varela J A, Longo E and Leite E R 2007 *Mater. Lett.* **61** 1904

[33] Liu Y H, Zuo J C, Ren X F and Yong L 2014 *Metalurgija* **53** 463

[34] Azaroff L V 1968 *Elements of X-ray crystallography* (New York: McGraw-Hill) p 552

[35] Orel Z and Orel B 1994 *Phys. Status Solidi B* **186** 33

[36] Brus L E 1984 *J. Chem. Phys.* **80** 4403

[37] Bueno R M, Martinez-Duart J M, Hernandez-Velez M and Vazquez L 1997 *J. Mater. Sci.* **32** 1861

[38] Patsalas P, Logothetidis S, Sygellou L and Kennou S 2003 *Phys. Rev. B* **68** 035104(1–13)

[39] Arote S, Ingle R, Tabhane V and Pathan H 2014 *J. Renew. Sust. Energy* **6** 013132(1–9)

[40] Singh S P, Roy M S, Thomas K R J, Balaiah S, Bhanuprakash K and Sharma G D 2012 *J. Phys. Chem. C* **116** 5941

[41] Liu G, Rodriguez J A, Hrbek J, Dvorak J and Peden C H F 2001 *J. Phys. Chem. B* **105** 7762